

SIT 45: An interacting, compact, and star-forming isolated galaxy triplet.

D. Grajales-Medina^{1,2}, M. Argudo-Fernández^{3,4,5}, P. Vázquez-Bustos⁵, S. Verley^{3,4}, M. Boquien⁶, S. Salim⁷,
S. Duarte Puertas^{8,9}, U. Lisenfeld^{3,4}, D. Espada^{3,4}, and H. Salas-Olave⁶

¹ Universidad Internacional de Valencia. Carrer del Pintor Sorolla 21, 46002, Valencia, Spain

² Facultad de Ingeniería, Departamento de Ciencias Básicas, Universidad Ean, Bogotá, Colombia

³ Departamento de Física Teórica y del Cosmos Universidad de Granada, 18071 Granada, Spain
e-mail: margudo@ugr.es

⁴ Instituto Universitario Carlos I de Física Teórica y Computacional, Universidad de Granada, 18071 Granada, Spain

⁵ Instituto de Física, Pontificia Universidad Católica de Valparaíso, Casilla 4059, Valparaíso, Chile.

⁶ Centro de Astronomía (CITEVA), Universidad de Antofagasta, Avenida Angamos 601 Antofagasta, Chile

⁷ Department of Astronomy, Indiana University, Bloomington, IN, 47404

⁸ Département de Physique, de Génie Physique et d'Optique, Université Laval, and Centre de Recherche en Astrophysique du Québec (CRAQ), Québec, QC, G1V 0A6, Canada

⁹ Instituto de Astrofísica de Andalucía - CSIC, Glorieta de la Astronomía s.n., 18008 Granada, Spain

Received ; accepted

ABSTRACT

Context. The underlying scenario of the formation and evolution of galaxy triplets is still uncertain. Mergers of galaxies in isolated triplets give us the opportunity to study the already complex merging process, with minimal contamination of other environmental effects that potentially allow and accelerate galaxy transitions from active star forming to passive galaxies.

Aims. The merging system SIT 45 (UGC 12589) is an unusual isolated galaxy triplet, consisting of three merging late-type galaxies, out of 315 systems in the SIT (SDSS-based catalogue of Isolated Triplets). The main aims of this work are to study its dynamical evolution and star formation history (SFH), as well as its dependence on its local and large-scale environment.

Methods. To study its dynamics, parameters such as the velocity dispersion (σ_v), the harmonic radius (R_H), the crossing time ($H_0 t_c$), and the virial mass (M_{vir}), along with the compactness of the triplet (S) were considered. To investigate the possible dependence of these dynamical parameters on the environment, the tidal force Q parameters (both local and large-scale) and the projected local density (η_k) were used. To constrain the SFH, we used CIGALE to fit its observed spectral energy distribution using multi-wavelength data from the ultraviolet to the infrared.

Results. SIT 45 is one of the most compact triplets in the SIT, and it is also more compact than triplets in other samples. According to its SFH, SIT 45 presents star-formation, where the galaxies also present recent (~ 200 Myr) star-formation increase, indicating that this activity may have been triggered by the interaction. Its dynamical configuration suggests that the system is highly evolved in comparison to the SIT. However this is not expected for systems composed of star-forming late-type galaxies, based on observations in compact groups.

Conclusions. We conclude that SIT 45 is a system of three interacting galaxies that are evolving within the same dark matter halo, where its compact configuration is a consequence of the on-going interaction, rather than due to a long-term evolution (as suggested from its $H_0 t_c$ value). We consider two scenarios for the present configuration of the triplet, one where one of the members is a tidal galaxy, and another where this galaxy arrives to the system after the interaction. Both scenarios need further exploration. The isolated triplet SIT 45 is therefore an ideal system to study short timescale mechanisms ($\sim 10^8$ years), such as starbursts triggered by interactions which are more frequent at higher redshift.

Key words. galaxies: general – galaxies: formation – galaxies: evolution – galaxies: interactions – galaxies: star formation

1. Introduction

It is difficult to overstate the importance of galaxy interactions on the evolution of galaxies across cosmic times. Over the past decades, great progress has been made to understand the mechanisms at play in the already complex case of galaxy pairs (Di Matteo et al. 2007; Ellison et al. 2010; Sales et al. 2012; Ellison et al. 2013, 2019; Patton et al. 2020; Maschmann et al. 2022). In general, galaxy mergers are an important mechanism affecting galaxies, and may lead to complex stellar populations, due to multiple starburst episodes (Kennicutt et al. 1987; Barton et al. 2000; Bergvall et al. 2003; McIntosh et al. 2008; D’Onghia et al. 2008; Yuan et al. 2012; Renaud et al. 2022). During galaxy in-

teractions, gas and stars are carried outside of their parent galaxies due to tidal forces or collisions between gas clouds (Toomre 1977; Barnes & Hernquist 1992; Naab et al. 1999, 2006; Ji et al. 2014; Dumont & Martel 2021). Tidal tails and bridges can form out of gas, sometimes in huge clouds, and stars can be found far away from their parent galaxies (de Mello et al. 2008; Duc & Renaud 2013; Pasha et al. 2021). In some particular cases leading to the formation of tidal dwarf galaxies (Duc & Mirabel 1994; Mendes de Oliveira et al. 2001; Neff et al. 2005; Bournaud & Duc 2006; Lelli et al. 2015).

Despite their importance, the exploration of the merging process in the even more complex, but also interesting case of

galaxy triplets have not been studied in detail, in contrast to close pairs or denser groups of galaxies (e.g., compact groups), where more extensive work has been done (Rubin et al. 1991; Zepf 1993; Moles et al. 1994; Coziol & Plauchu-Frayn 2007; Renaud et al. 2009; Ellison et al. 2011; Torres-Flores et al. 2014; Wild et al. 2014; Vogt et al. 2015). According to Heidt et al. (1999), strongly interacting galaxy triplets may be responsible for the formation of a BL Lac object. Reshetnikov et al. (2006) found a connection between the physical properties of a galaxy triplet and the formation of a giant spiral polar ring galaxy, another peculiar object, from tidal transfer of mass from the other two member galaxies. A possible on-going triple galaxy merger was found in Hickson compact group 95 (HCG 95) by Iglesias-Páramo & Vílchez (1997), nevertheless since this is happening in a group, it can not be strictly compared with a merger in a galaxy triplet.

From the point of view of simulations, adding a third galaxy greatly increases the number of possible scenarios in their formation and evolution, making their study considerably more challenging (Agekyan & Anosova 1968; Aceves 2001). However, galaxy triplets would be the simplest system to figure out the behaviour in more complex ones such as compact groups, where gas can be expelled by the collisions to the intergalactic medium and it can interact with other member galaxies (Gao & Xu 2000; Lisenfeld et al. 2002, 2004). On the contrary, galaxy triplets are generally located in low-density environments, where the in-situ interaction between the members would be the main process driving their evolution (Costa-Duarte et al. 2016). This has been also observed in compact groups, as in the Stephan’s Quintet (Duarte Puertas et al. 2019). In addition, the study of isolated merging triplets gives us the possibility to segregate the merging process itself. That is, to separate it from other environmental effects which could enable and accelerate galaxy transitions from actively star forming to quiescent galaxies, such as ram-pressure stripping of the cold interstellar medium (Gunn & Gott 1972), the removal of the hot gas halo, also known as ‘strangulation’ (Larson et al. 1980; Balogh & Morris 2000), or fast encounters with other galaxies (or galaxy ‘harassment’, see also Gallagher & Ostriker 1972; Moore et al. 1996, 1998).

Galaxy triplets are not common objects in the local Universe. The expected number of triplet galaxy mergers occurring at the present epoch is very low ($< 10\%$ of galaxy triplets, Aceves 2001), however some effort has been done to identify and characterise the observational and dynamical properties of these unusual objects (Karachentseva et al. 1979; Karachentseva & Karachentsev 2000). The advent of large photo-spectroscopic surveys, such as the Sloan Digital Sky Survey (SDSS; York et al. 2000; Aguado et al. 2019), has allowed us to better characterise these systems (Elyiv et al. 2009; Hernández-Toledo et al. 2011; O’Mill et al. 2012; Argudo-Fernández et al. 2015b), and therefore better understand their formation and evolution (Duplancic et al. 2013, 2015; Costa-Duarte et al. 2016; Tawfeek et al. 2019). The largest sample of spectroscopically selected galaxy triplets is composed of about one thousand systems (O’Mill et al. 2012). Nevertheless, isolated triplets are even more rare and amount to 315 in the local Universe (Argudo-Fernández et al. 2015b). These isolated triplets (i.e., with no physical neighbour within a projected distance of 1 Mpc and line-of-sight velocity difference $\Delta v \leq 500 \text{ km s}^{-1}$) compose the SDSS-based catalogue of Isolated Triplets (hereafter SIT). The SIT was compiled by Argudo-Fernández et al. (2015b), based on the tenth data release of the SDSS (SDSS-DR10, Ahn et al. 2014) and it represents about 3% of the total number of galaxies in SDSS spectroscopic sample.

The isolated triplet SIT 45 ($z=0.034$, $\sim 145 \text{ Mpc}$), also known as UGC 12589, is a major ‘wet’ merger, i.e. a merger between similar mass, gas-rich, and blue late-type galaxies, involving three member galaxies. Wet mergers are found to be more prominent in low-density environments (Bekki et al. 2001; Sánchez-Blázquez et al. 2009; Lin et al. 2010). However, we have only found 9 ongoing mergers in the SIT ($< 3\%$ of the SIT), where only 3 of them can be classified as wet mergers, including SIT 45. This number is even slower than expected according to Aceves (2001). SIT 45 is therefore an ideal and relatively unique object to study wet mergers in an extremely low density environment. The existence of these kind of systems can be considered as a consequence of structure formation, which happens more slowly and at smaller scales than in regions with average density, and a possible pathway for the formation of gas rich disks (Chengalur et al. 2016).

Given that SIT 45 is a system consisting of three interacting galaxies, it is expected to show a complex dynamics and star formation history (SFH). We therefore focus this work on the study of the evolution of SIT 45 through its dynamic properties and configuration, as well as depending on its local environment and large-scale structure (LSS). We also investigate its SFH using multi-wavelength data, from the ultraviolet (UV) to the mid-infrared (MIR). This study is organised as follows. In Sec. 2 we describe in detail the isolated triplet SIT 45 and some of its properties in comparison with the SIT (including environment), as well as the dynamical parameters used in this study and the data used to get its spectral energy distribution (SED) to constrain its SFH. We present our results in Sec. 3 and the associated discussion in Sec. 4. Finally, a summary and the main findings of the study are presented in Sec. 5. Throughout the study, a cosmology with $\Omega_{\Lambda_0} = 0.7$, $\Omega_{m_0} = 0.3$, and $H_0 = 70 \text{ km s}^{-1} \text{ Mpc}^{-1}$ is assumed.

2. Data and methodology

2.1. The unusual system SIT 45

According to the NASA/IPAC Extragalactic Database (NED¹), SIT 45 (UGC 12589) was initially classified as a galaxy pair (de Vaucouleurs et al. 1991), composed of SIT 45B and SIT 45C separated by a projected distance of $\sim 52 \text{ kpc}$. However Argudo-Fernández et al. (2015b) noted the existence of SIT 45A, at a projected distance of $\sim 17 \text{ kpc}$ from SIT 45B (as shown in Fig. 1). The line of sight velocity difference between SIT 45A and SIT 45B is $\Delta v \simeq 118 \text{ km s}^{-1}$, and $\Delta v \simeq 104 \text{ km s}^{-1}$ between SIT 45A and SIT 45C, with a projected separation of $d \simeq 64 \text{ kpc}$.

Table 1 shows general properties of the galaxies composing SIT 45: coordinates, redshift, apparent size, and absolute magnitudes.

Galaxies in the SIT were selected from a volume—limited sample of galaxies in the SDSS-DR10 in the redshift range $0.005 \leq z \leq 0.080$ and apparent magnitude $11 \leq m_r \leq 15.7$, where m_r is the SDSS *model* magnitude in *r* band. The SIT is composed of 315 physically bound isolated triplets within a projected distance up to $d \leq 450 \text{ kpc}$ with a light-of-sight velocity difference $\Delta v \leq 160 \text{ km s}^{-1}$. More details about the criteria to select physically bound systems can be found in Argudo-Fernández et al. (2015b). Note that galaxies in the SIT are named according to their m_r apparent magnitude, with galaxy A (or central galaxy) the brightest and galaxy C the faintest.

¹ <https://ned.ipac.caltech.edu/>

(1) Galaxy	(2) RA (deg)	(3) DEC (deg)	(4) z	(5) r_{90} (arcsec)	(6) (M_u, M_g, M_r, M_i, M_z) (abs mag)
SIT 45A	23:25:00.25	-00:00:08.1	0.03358	28.51	(-19.37,-20.11,-20.39,-20.45,-20.43)
SIT 45B	23:25:01.84	-00:00:01.5	0.03397	26.03	(-18.85,-19.62,-20.00,-20.21,-20.04)
SIT 45C	23:25:03.81	+00:01:07.2	0.03392	1.44	(-16.69,-17.52,-18.18,-18.59,-18.84)

Table 1. General properties of SIT 45. The columns correspond to: (1) name of the galaxy in SIT 45; (2) J2000.0 right ascension in degrees; (3) J2000.0 declination in degrees; (4) redshift of the galaxy; (5) Petrosian radius containing 90% of the total flux of the galaxy in the r -band; (6) absolute magnitude in the SDSS-DR10 (u, g, r, i, z) bands. Galaxy coordinates, redshift, and r_{90} data are from the SDSS-DR10. The absolute magnitudes were obtained by fitting the spectral energy distribution in the five bands of the SDSS-DR10 using the k-correct routine (Blanton & Roweis 2007).

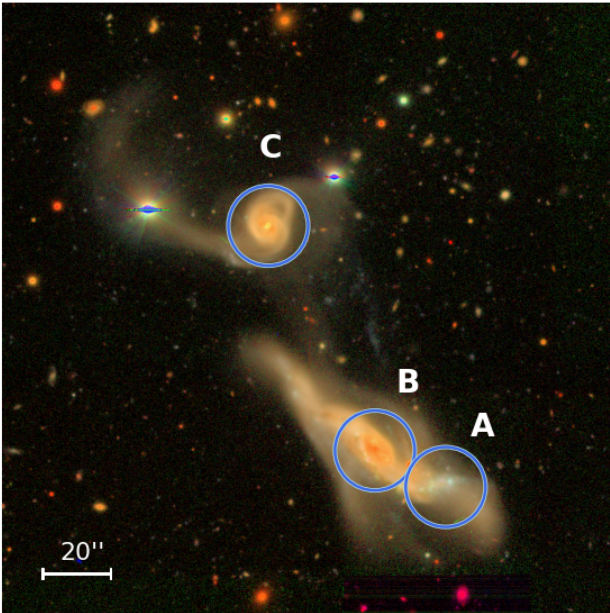


Fig. 1. Hyper Suprime-Cam (HSC, Aihara et al. 2022) g-r-i band colour image of the isolated triplet SIT 45 (UGC 12589). North is up and east is left. The A, B, and C galaxies are marked in their central region with a light blue circle and the corresponding letter. The 20'' scale of the image corresponds to 0.4 arcsec per pixel, with a total physical extent of ~ 170 kpc.

2.2. Multiwavelength UV to IR broadband SED fitting

We used multiwavelength photometry, from the ultraviolet (UV) to infrared (IR), to derive the panchromatic spectral energy distribution (SED) for SIT 45. In combination with models, the SED of a galaxy is a powerful tool to constrain key physical properties of the unresolved stellar populations (Walcher et al. 2011). The UV data were taken from the Galaxy Evolution Explorer (GALEX) satellite All Sky Survey (Martin et al. 2005). In particular, we used the photometry with the deepest depth of UV observations, both in the far-UV (FUV), at 1528 Å, and the near-UV (NUV), at 2271 Å. The optical comes from the SDSS-DR10 photometry in the five SDSS bands: u (3551 Å), g (4686 Å), r (6166 Å), i (7480 Å), and z (8932 Å). The IR photometry comes from the Wide-field Infrared Survey Explorer (WISE; Wright et al. 2010). In particular we used the unofficial unblurred coadds of the WISE imaging (unWISE; Lang et al. 2016), which provide significantly deeper imaging while preserving the resolution of the original WISE images. We used the W1, W2, and

W3 WISE bands, centred at 3.4, 4.6, and 12 μm , respectively. We also used near-infrared (NIR) photometry from the Two Micron All Sky Survey (2MASS; Skrutskie et al. 2006). The cutout images of the galaxies in SIT 45 in each band are shown in Fig. 2. In order to combine the photometry in the different bands, we used the high resolution convolution kernels developed by Aniano et al. (2011) to convolve to the instrumental point-spread function (PSF) of the W3 band ($\text{PSF} \approx 6''$).

We used CIGALE² (Code Investigating GALaxy Emission; Burgarella et al. 2005; Noll et al. 2009; Boquien et al. 2019) to perform the UV to IR broadband SED fitting, since it is a code specifically developed to study galaxy emission taking into account both the UV/optical dust attenuation as well as its re-emission in the infrared. Hence, this code has been widely used in the literature to derive star formation rate (SFR), star formation history (SFH) and, dust attenuation in galaxies from the multi-wavelength SED UV to IR (Buat et al. 2011; Giovannoli et al. 2011; Boquien et al. 2014; Ciesla et al. 2017; Yuan et al. 2018; Boquien et al. 2022). A detailed description of the code can be found in Boquien et al. (2019).

Given the nature of SIT 45, we assumed a delayed SFH with optional constant burst/quench as explained in Ciesla et al. (2017). They expanded the delayed SFH allowing for an instantaneous recent variation of the SFR, which is flexible to model star-forming galaxies inside the scatter of the main sequence (Noeske et al. 2007; Elbaz et al. 2011), but also starbursts and rapidly quenched galaxies (Ciesla et al. 2016). This is therefore one of the most simple methods to model the SFH of interacting galaxies, inasmuch as it considers an older stellar population with an upward or downward recent variation of the SFH, setting it to a constant until the last time step. This module is provided as `sfhdelayedbq` in CIGALE (see Boquien et al. 2019, for details).

To compute the analytic SFH, we adopt the single stellar populations of Bruzual & Charlot (2003), hereafter BC03, considering a Salpeter IMF (Salpeter 1955), and a fixed value of the stellar metallicity $Z = 0.02$ (solar metallicity) to model the non-attenuated stellar emission. The energy absorbed by the dust, considering a modified version of the dust attenuation model of Calzetti et al. (2000) with a flexible attenuation curve (Noll et al. 2009), is re-emitted in the IR using the dust emission templates of Dale et al. (2014), without considering AGN contribution. Note that we have checked that galaxies in SIT 45 are non AGNs using the analysis of Brinchmann et al. (2004) on SDSS spectra. The values of the different parameters we used to create a set of SED models are listed in Table 2. These are the parameters used in CIGALE to model the SFH, dust attenuation, and dust emission. With these parameters we modelled 1 088 640 different SEDs. Note that with the Bayesian analysis

² <https://cigale.lam.fr/>

performed by CIGALE, we do not select as the best model the one that minimises the chi squared fitting. We therefore provide mean values, and their uncertainties, weighted by the probability density function of all the models.

2.3. Quantification of the environment

Argudo-Fernández et al. (2015b) provided two parameters to quantify the effects of the local and the LSS environment on each isolated triplet: the tidal strength parameter (Q) and the projected number density (η_k). The combination of these two complementary parameters describes the environment around galaxies (Verley et al. 2007; Sabater et al. 2013; Argudo-Fernández et al. 2013, 2014).

The Q parameter of a galaxy is equivalent to the sum of the individual ratios $\frac{F_{\text{tidal}}}{F_{\text{bind}}}$ of the external tidal force exerted by each neighbouring galaxy (F_{tidal}), with respect to its internal binding force (F_{bind}). The Q for a galaxy P is defined by the equation (Verley et al. 2007; Argudo-Fernández et al. 2013):

$$Q \propto \log \left[\sum_i \frac{M_{\star i}}{M_{\star P}} \left(\frac{D_P}{d_i} \right)^3 \right], \quad (1)$$

where $M_{\star i}$ and d_i are the stellar mass and the projected physical distance of the considered i^{th} neighbour, $M_{\star P}$ and D_P are the stellar mass and apparent diameter of galaxy P, where $D_P = 2\alpha r_{90}$ following the empirical calibration in Argudo-Fernández et al. (2013), with $\alpha = 1.43$ and r_{90} the Petrosian radius containing the 90% of the total flux of the galaxy.

To consider the local environment, Argudo-Fernández et al. (2015b) quantified the effect of galaxies B and C on galaxy A ($Q_{A,\text{trip}}$). As we can observe in the case of SIT 45, the brightest galaxy in the system is not always the most massive. We therefore use the Q_{trip} parameter as defined in Vázquez-Bustos et al. (in preparation), which provides a more complete information of the tidal strengths in galaxy triplets. It not only considers $Q_{A,\text{trip}}$, but also the total tidal strengths exerted on the B ($Q_{B,\text{trip}}$) and the C ($Q_{C,\text{trip}}$) galaxies as follows:

$$Q_{\text{trip}} = \frac{Q_{A,\text{trip}} + Q_{B,\text{trip}} + Q_{C,\text{trip}}}{3}. \quad (2)$$

For the LSS environment, Argudo-Fernández et al. (2015b) considered galaxies within a volume of $\Delta v \leq 500 \text{ km s}^{-1}$ from 1 to 5 Mpc projected radius, that is neighbouring galaxies at distances larger than the isolation criteria definition of the triplets up to 5 Mpc, defining a Q_{LSS} parameter.

The projected number density ($\eta_{k,\text{LSS}}$) is used to characterise the LSS surrounding each isolated triplet, and is defined as:

$$\eta_{k,\text{LSS}} \equiv \log \left(\frac{k-1}{\text{Vol}(d_k)} \right) = \log \left(\frac{3(k-1)}{4\pi d_k^3} \right), \quad (3)$$

where d_k is the projected physical distance to the k^{th} nearest neighbour, with k equal to 5, or less, if there are not enough neighbours in the field out to a projected distance of 5 Mpc.

According to Argudo-Fernández et al. (2013, 2014), the most isolated systems with respect to the LSS environment (i. e. very isolated triplets from any external influence) show low values of $\eta_{k,\text{LSS}}$ and Q (either Q_{trip} or Q_{LSS}). On the contrary, less isolated systems show higher values of these parameters, since they may be affected by perturbations generated by the existence of neighbours in the LSS. Additionally, a galaxy triplet with an average

$\eta_{k,\text{LSS}}$ and high Q_{trip} is surely presenting on-going strong interaction/mergers. For average $\eta_{k,\text{LSS}}$, it could be also likely identified as a compact triplet if this is presenting a high Q_{LSS} . Note that the Q parameter is not a measurement of the compactness of a system, but more an indicator of its degree of interaction or isolation.

When working with isolated galaxies or galaxy groups, Argudo-Fernández et al. (2015b, 2016) have shown that these parameters can be used to identify if the system is mainly located in a void environment (low values of Q_{LSS}), or on the contrary, it is closer to the outskirts of larger structures, such as walls, filaments, or clusters, with higher values of Q_{LSS} .

2.4. Dynamical parameters

To characterise the dynamics of SIT 45 we have used a series of parameters that are usually defined to study the dynamics of clusters of galaxies or compact groups, and which can also be applied to small galaxy groups, such as triplets (Vavilova et al. 2005; Elyiv et al. 2009). The dynamical parameters used in this work are the projected mean harmonic radius, R_H ; the velocity dispersion of the triplet, σ_v ; the dimensionless crossing time, $H_0 t_c$; and the virial mass of the triplet, M_{vir} . These parameters are defined as follows.

The parameter R_H is an estimation of the size of the halo of a galaxy group or cluster. It measures the effective radius of its gravitational potential, independently of the location of the centre of the system. The parameter is defined by the equation (Araya-Melo et al. 2009):

$$R_H = \left(\frac{1}{N} \sum R_{ij}^{-1} \right)^{-1}, \quad (4)$$

where R_{ij} is the projected distance between the galaxies of the system, in kpc, and N is the number of galaxies ($N = 3$). According this definition, R_H is mainly based on the projected separation between the triplet members, indicating whether they are close to each other (that is, its compactness) or far from each other (that is, if the system is a loose group). Therefore, R_H is independent of the location of the triplet centre, allowing it to reflect the internal structure of the system (Araya-Melo et al. 2009; White et al. 2015).

Velocity dispersion in galaxy groups and clusters commonly form the basis for dynamical estimates of their mass using the virial theorem (Beers et al. 1990). In the present study we used the (line-of-sight) velocity dispersion, $\sigma_{v_{\text{los}}}$, defined as (Duplancic et al. 2015):

$$\sigma_{v_{\text{los}}}^2 = \frac{1}{N-1} \sum (v_r - \langle v_r \rangle)^2, \quad (5)$$

where v_r is the line-of-sight velocity, and $N = 3$. Under this definition, the velocity dispersion of the triplet is an estimation of how fast member galaxies move between each other. It is important to note that projection effects might be important. We therefore estimated the three-dimensional velocity dispersion (used in the computation of the dynamical parameters $H_0 t_c$ and M_{vir} , as shown below) as $\sigma_{v_{3D}}^2 = 3\sigma_{v_{\text{los}}}^2$. Hereafter we generally use σ_v to refer to $\sigma_{v_{\text{los}}}$.

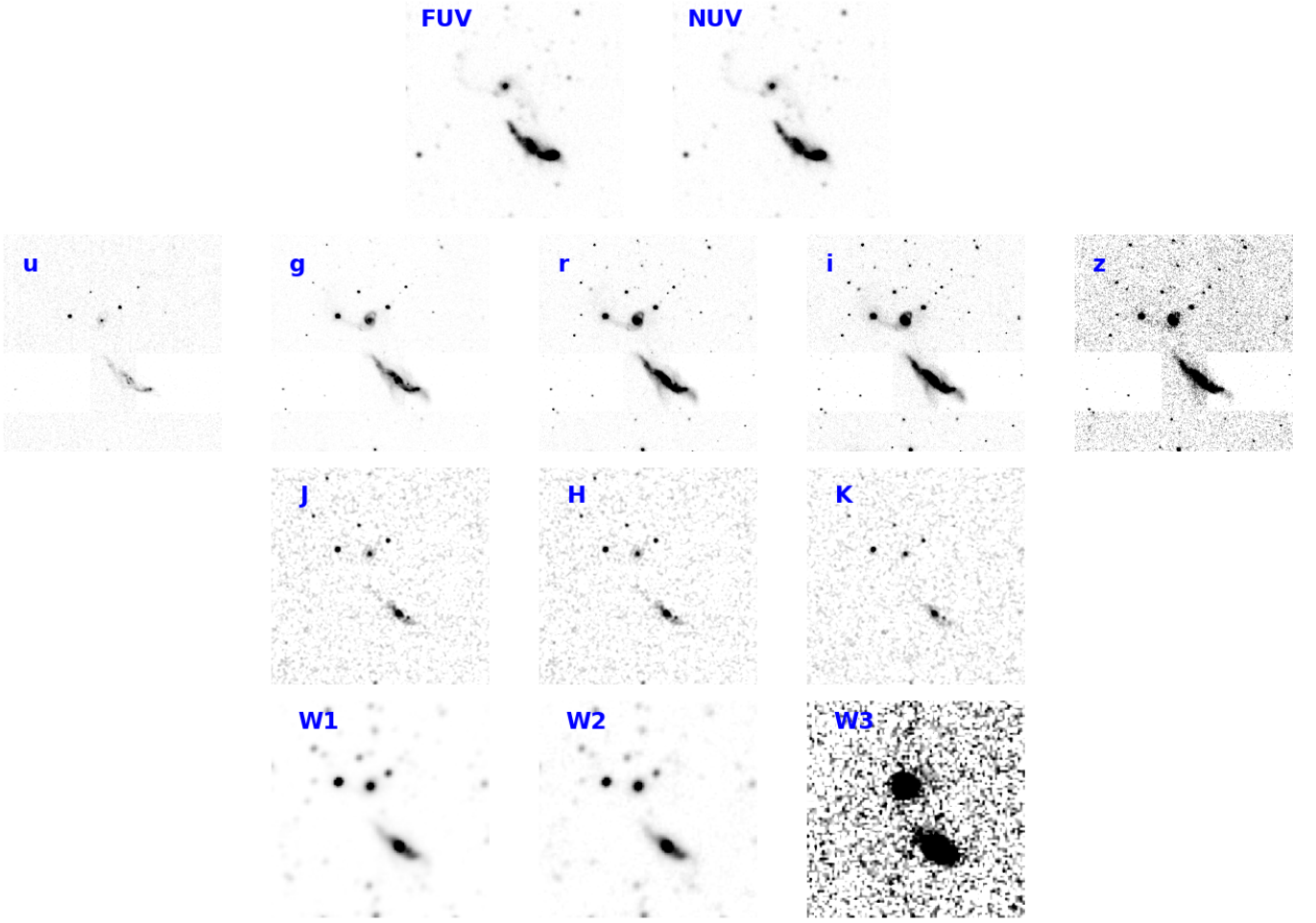


Fig. 2. Multiwavelength (UV-optical-NIR) 4 arcmin² FoV images of SIT 45. GALEX (FUV and NUV), SDSS (u, g, r, i, and z), 2MASS (J, H, and K), and unWISE (W1, W2, and W3) are presented from left upper to right lower panels, respectively. All the images are rotated north-up and east-left.

Following the work of [Hickson et al. \(1992\)](#), for compact groups of galaxies, the dimensionless crossing time parameter, $H_0 t_c$, and the virial mass, M_{vir} , are defined by the equations:

$$H_0 t_c = H_0 \frac{4R_H}{\sqrt{3}\pi\sigma_v} \quad (6)$$

and

$$M_{\text{vir}} = \frac{3\pi R_H \sigma_v^2}{2G} \quad (7)$$

with G is the gravitational constant. According to [Hickson et al. \(1992\)](#), $H_0 t_c$ is the ratio of the crossing time to the age of the universe, where its reciprocal is related to the maximum number of times a galaxy could have traversed the group since its formation.

In addition to these parameters, we have estimated the compactness of the triplet, S , to have a measurement of the spatial configuration of the galaxies in SIT 45, complementary with the parameter R_H . The compactness is a physical property that measures the percentage of the total area that is filled with the light of the galaxies composing the triplet. This parameter S is defined as:

$$S = \frac{\sum_{i=1}^3 r_{90}^2}{r_m^2} \quad (8)$$

where r_m is the minimum radius of the circle containing the geometrical centres of the three galaxies in triplets ([Duplancic et al. 2013](#)). We used these parameters to compare SIT 45 to other triplets in the SIT.

3. Results

3.1. Star formation history of SIT 45

As mentioned in Sec. 2.2, we used CIGALE to constrain the SFH of the isolated triplet SIT 45 using the set of values presented in Table 2 fitting the observed SED from the UV to the IR. Since SIT 45A and SIT 45B are overlapping in the same area, it is difficult to separate the photometry contribution of each galaxy. We therefore perform the SED fitting to all the pixels within an area of 4 arcmin² around the system for each band, obtaining surface densities of the properties of the unresolved stellar populations. In particular, we use the the SFR surface density (Σ_{SFR}) map presented in Fig. 3 to select the pixels corresponding to the A, B, and C galaxies.

We use the *astrodendro*³ Python package to perform a 'dendrogram' (hierarchical tree-diagram) analysis of the resulted SFR surface density map (as shown in Fig. 3). A dendrogram graphically represents the hierarchical structure of nested iso-surfaces, which is particularly useful for analysing astronomical

³ <http://www.dendrograms.org/>

Model	Parameter	value
SFH	Age (Myr)	11000, 12000, 13000
	τ_{main} (Myr)	1000, 3000, 5000, 7000, 9000
	Age _{bq} (Myr)	20, 50, 100, 300
	r_{SFR}	0, 0.25, 0.5, 0.75, 1, 1.5, 2, 5, 10
Dust attenuation	$E(B - V)_{\text{lines}}$ (mag)	0.05, 0.10, 0.15, 0.20, 0.25, 0.30, 0.35, 0.40, 0.45, 0.50, 0.55, 0.60, 0.65, 0.70, 0.75, 0.8
	$E(B - V)_{\text{factor}}$	0.25, 0.5, 0.75
	UV bump wavelength (nm)	217.5
	UV bump width (nm)	35.0
	UV bump amplitude	0.0, 1.5, 3.0
	$\Delta\delta$	-1.0, -0.9, -0.8, -0.7, -0.6, -0.5, -0.4, -0.3, -0.2, -0.1, 0, 0.1, 0.2, 0.3
Dust emission	α	2.0

Table 2. Parameters used in CIGALE to model the SFH (upper rows), dust attenuation (middle rows), and dust emission (lower row). Meaning of the parameters: a) SFH: Age – Age of the main stellar population in the galaxy, in Myr; τ_{main} – e -folding time of the main stellar population model, in Myr; Age_{bq} – Age of the burst/quench episode, in Myr; and r_{sfr} – Ratio of the SFR after/before Age_{bq}, values larger than one correspond to an enhancement of the SFR whereas values lower than one will correspond to a decrease; b) Dust attenuation: $E(B - V)_{\text{lines}}$ – Colour excess of the nebular lines light for both the young and old population; $E(B - V)_{\text{factor}}$ – Reduction factor to apply on $E(B - V)_{\text{lines}}$ to compute $E(B - V)_s$, the stellar continuum attenuation. Both young and old populations are attenuated by $E(B - V)_s$; UV bump wavelength – Central wavelength of the UV bump in nm; UV bump width – Width (FWHM) of the UV bump in nm; UV bump amplitude – Amplitude of the UV bump. For the Milky Way: 3; $\Delta\delta$ – Slope delta of the power law modifying the attenuation curve. c) Dust emission module: α – α slope in the Dale et al. (2014) model.

data (Rosolowsky et al. 2008; Goodman et al. 2009). The resulted mask for each galaxy is represented by orange contours. Note the difference with the contours using the same methodology but applied to photometry (represented by cyan and red contours, see image description). The parameters found for the SFH of each galaxy are shown in Table 3, following a Bayesian analysis and integrating the pixels corresponding to each galaxy to get total values of the parameters.

In general, the uncertainties found for the parameters are high, suggesting that the parameters of the SFH might be degenerate. However, the results are consistent with the spectroscopic classification of the galaxies in Brinchmann et al. (2004) using SDSS spectra. In addition, we also run CIGALE including emission line measurements from the Max Planck Institute for Astrophysics and Johns Hopkins University (MPA-JHU⁴; Kauffmann et al. 2003; Tremonti et al. 2004; Salim et al. 2007) added value catalogue (Brinchmann et al. 2004) with spectroscopic reanalysis of the optical SDSS spectra of the galaxies (shown in Fig. 4). In particular, we used emission line fluxes H_α and H_β , with the D4000 break parameter using the Balogh et al. (1999), in combination with fiber SDSS magnitudes, using CIGALE. We found that the results for the SFR are consistent among them, as shown in Table 4, with some discrepancies in the stellar mass estimation, as can be observed in Fig. 5, which is a consequence of using information limited to the optical range and aperture effects.

To compare with the SIT, we use the GALEX-SDSS-WISE Legacy Catalog (GSWLC; Salim et al. 2016), which provides SFRs for 700,000 low-redshift ($0.01 < z < 0.30$) galaxies in the SDSS. The GSWLC also used CIGALE to derive SFR. There are three versions of the catalogue (GSWLC-A, M, D), depending on the depth of the UV photometry. In particular we use the GSWLC-2 catalogue (Salim et al. 2018), which has more accurate SFRs from joint UV+optical+MIR SED fitting, with the medium depth of the UV photometry, hence the GSWLC-M2 catalogue. We found SFRs for 470 galaxies in the SIT (including SIT 45, as shown in Fig. 5, where we show the values for all SIT galaxies in the GSWLC-M2 catalogue).

⁴ Available at <http://www.mpa-garching.mpg.de/SDSS/DR7/>

In Table 4 we present the obtained SFR for each galaxy in SIT 45 in comparison with the values reported in the GSWLC-M2 catalogue. The values of the SFR are fairly similar for galaxy SIT 45C, but there is some discrepancy for galaxies SIT 45A and SIT 45B, as it can be appreciated in the SFR- M_\star diagram in Fig. 5. These differences may be due in part because of the different input photometry and the different SED fitting priors (for instance different IMF), but mainly due to the different methodology. The GSWLC-M2 catalogue considers a two-exponentially decreasing function to take into account the contribution of a late star-formation burst event due the interaction of the member galaxies. In addition, given that galaxy SIT 45A looks overlapping SIT 45B from our point of view, it is difficult to separate the photometry contribution of each galaxy to analyse them. For this reason we use the resulted SFR map to identify the contribution of each galaxy (orange contours in Fig. 3), instead of using photometry (cyan and red contours in Fig. 3).

Note also that the stellar mass for galaxy SIT 45B from UV-to-NIR SED fitting ($\log(M_\star) = 10.29 M_\odot$) is larger than the stellar mass provided in the GSWLC-M2 catalogue, which is based on photometry for all the galaxies in the SIT (see the Fig. 5).

3.2. Environment of SIT 45

We used stellar masses obtained from UV-to-NIR SED fitting and the values of the apparent diameters in Table 1 to estimate the Q_{trip} parameter for SIT 45 following Eq. 2. We found a value of $Q_{\text{trip}} = -0.09 \pm 0.09$, which is one of the highest values for the SIT, with mean value $Q_{\text{trip}} = -2.14$ and standard deviation 0.83. This result is expected given the fact that SIT 45 is a merging system.

According to the quantification of the LSS environment for isolated triplets in Argudo-Fernández et al. (2015b), SIT 45 presents a higher value of the tidal parameter due to the LSS environment ($Q_{\text{LSS}} = -3.31$) than the rest of the SIT (with a mean value of $Q_{\text{LSS}} = -5.05$ and standard deviation 0.71). This is mainly due to SIT 45 having 28 LSS associated galaxies, meanwhile the mean value in the SIT is 25. However the nearest neighbour is found at a projected distance $d_{\text{nn}} = 2.26$ Mpc (where the mean value for the SIT is $d_{\text{nn}} = 1.42$ Mpc). The value of its

(1) Galaxy	(2) τ_{main} (Myr)	(3) Age_{bq} (Myr)	(4) r_{SFR}	(5) SFR ($M_{\odot}\text{yr}^{-1}$)	(6) SFR ₁₀₀ ($M_{\odot}\text{yr}^{-1}$)	(7) $\log(M_{\star})$ (M_{\odot})
SIT 45A	7063 ± 1447	116 ± 102	1.7 ± 0.7	0.51 ± 0.10	0.50 ± 0.11	9.70 ± 0.04
SIT 45B	5302 ± 1719	217 ± 108	0.3 ± 0.4	0.31 ± 0.15	0.45 ± 0.24	10.29 ± 0.05
SIT 45C	6826 ± 1776	213 ± 84	5.3 ± 1.9	2.62 ± 0.38	2.30 ± 0.44	9.84 ± 0.08

Table 3. Parameters found for the SFH of SIT 45 following a Bayesian analysis as provided by CIGALE using photometry from the UV-to-NIR. The columns correspond to: (1) galaxy in the triplet SIT 45; (2) e -folding time of the main stellar population model, in Myr; (3) age of the burst/quench, in Myr; (4) ratio of the SFR after/before Age_{bq} ; (5) star formation rate, in $M_{\odot}\text{yr}^{-1}$; (6) average SFR over 100 Myr, in $M_{\odot}\text{yr}^{-1}$; (7) stellar mass, in M_{\odot} . Intensive parameters of the SFH (τ_{main} , Age_{bq} , and r_{SFR}) are luminosity weighted.

(1) Galaxy	(2) $\log(\text{SFR})_{\text{GSWLC}}$ $M_{\odot}\text{yr}^{-1}$	(3) $\log(\text{SFR})_{\text{UV-to-NIR}}$ $M_{\odot}\text{yr}^{-1}$	(4) $\log(\text{SFR})_{\text{fiber}}$ $M_{\odot}\text{yr}^{-1}$
SIT 45A	0.277 ± 0.077	-0.290 ± 0.083	-0.534 ± 0.148
SIT 45B	0.283 ± 0.079	-0.516 ± 0.206	-0.155 ± 0.127
SIT 45C	0.391 ± 0.035	0.418 ± 0.064	0.442 ± 0.068

Table 4. SFR for the galaxies in SIT 45. The columns correspond to: (1) Galaxy name; (2) SFR in the GSWLC-M2 catalogue (Salim et al. 2018); (3) SFR in this work using photometry from UV to NIR; (4) SFR in this work combining photometry (fiber magnitude) and optical SDSS spectra.

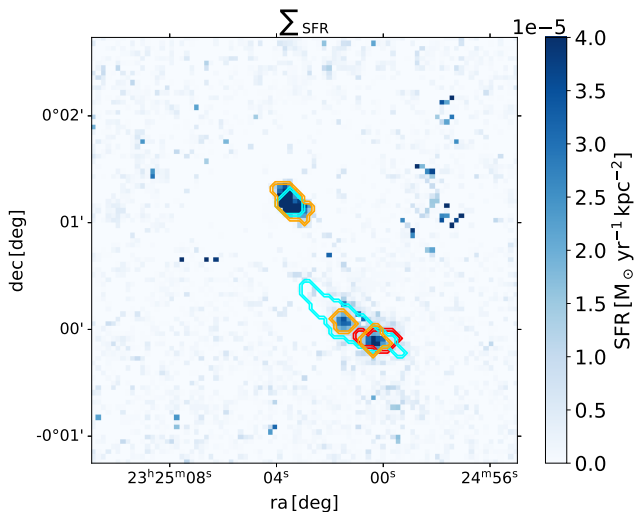


Fig. 3. SFR surface density (Σ_{SFR}) map obtained for the isolated triplet SIT 45 in a 4 arcmin² FoV, North is up, East is left. Coordinates are given in J2000. Colour bar is normalised to show the mean value for all the pixels within 5σ . Orange contours correspond to the mask defined on the Σ_{SFR} map using astrodendro. For an easiest comparison, we show the contours corresponding to the A galaxy (red contour) and the B and C galaxies (cyan contours). White contours were defined as astrodendro masks on a high resolution three-colour (g,r,i) image from the Hyper Suprime-Cam of the Subaru telescope (Aihara et al. 2022) of SIT 45, (as shown in Fig. 1). The red contour corresponding to the A galaxy selected using the GALEX FUV image (as shown in the upper left panel of Fig. 2).

projected density ($\eta_{k,\text{LSS}} = -1.20$) is comparable with the rest of the SIT with mean value $\eta_{k,\text{LSS}} = -1.24$ and standard deviation 0.47. This suggests that even if SIT 45 is an isolated triplet, it might be influenced by the LSS. We have checked with the LSS-GalPY (Argudo-Fernández et al. 2015a, 2017) tool that there is a small cluster (i.e. structure composed of ~ 100 galaxies at the intersection of two filaments) at a projected distance $d \sim 2.49$ Mpc from SIT 45. This means that SIT 45 might be accreting of cold gas from the LSS, that could trigger nuclear activity or star for-

mation in the centre of the galaxies, depending on their stellar mass (Sabater et al. 2013; Argudo-Fernández et al. 2016, 2018).

The value of Q_{trip} for SIT 45 is about five orders of magnitude higher than Q_{LSS} , as expected since the galaxies are in interaction. This means that the effect of the LSS environment is negligible in comparison to the tidal strength due to the triplet member galaxies. This value is also higher than for most of the SIT triplets, also a consequence of the interaction of the galaxies and the fact that mergers are relatively unusual in isolated triplets (nine triplets out of 315), as previously introduced in Sec. 1.

Note that the size on SIT 45C is smaller than expected from Fig. 1, as well as SIT 45A has a size that is comparable to that of SIT 45B. SIT 45C is a galaxy with a bright stellar nucleus, therefore its measured Petrosian flux misses most of the extended light of the object and its Petrosian radius is set by its nucleus alone (Blanton et al. 2001; Yasuda et al. 2001). In the case of SIT 45A, its apparent size is overestimated due to the difficulty of separating the photometry for overlapping galaxies. According to Eq. 1, the smaller the apparent diameter the higher Q parameter, therefore the values of Q_{trip} and Q_{LSS} are underestimated by ~ 0.2 dex. This discrepancy does not have any effect on our results and conclusions, since we have checked that the nine SIT triplets with ongoing mergers have $Q_{\text{trip}} > -0.5$ (Vásquez-Bustos et al. in preparation), with SIT 45 one of the four triplets with the highest Q_{trip} , as shown in Fig. 7.

3.3. Dynamics and configuration of SIT 45

We used the dynamical parameters projected harmonic radius, R_H ; velocity dispersion, σ_v ; crossing time, $H_0 t_c$; and virial mass of the triplet, M_{vir} , described in Sec. 2.4 to study the dynamics of SIT 45 in a cosmological scenario where the system is built in a common primordial dark matter halo. As mentioned, we also used the compactness S to study the configuration of the triplet. The values of these parameters for SIT 45 are shown in Table 5. Figure 6 shows the dynamical parameters of SIT 45 in comparison with the distributions for the rest of the triplets in the SIT using statistical violin plots.

As can be seen in Fig. 6, the value of σ_v for SIT 45 ($\sigma_v = 64.43 \pm 0.65 \text{ km s}^{-1}$) is slightly higher than the median value in the SIT ($\sigma_v = 53.9 \text{ km s}^{-1}$) but inside the interquar-

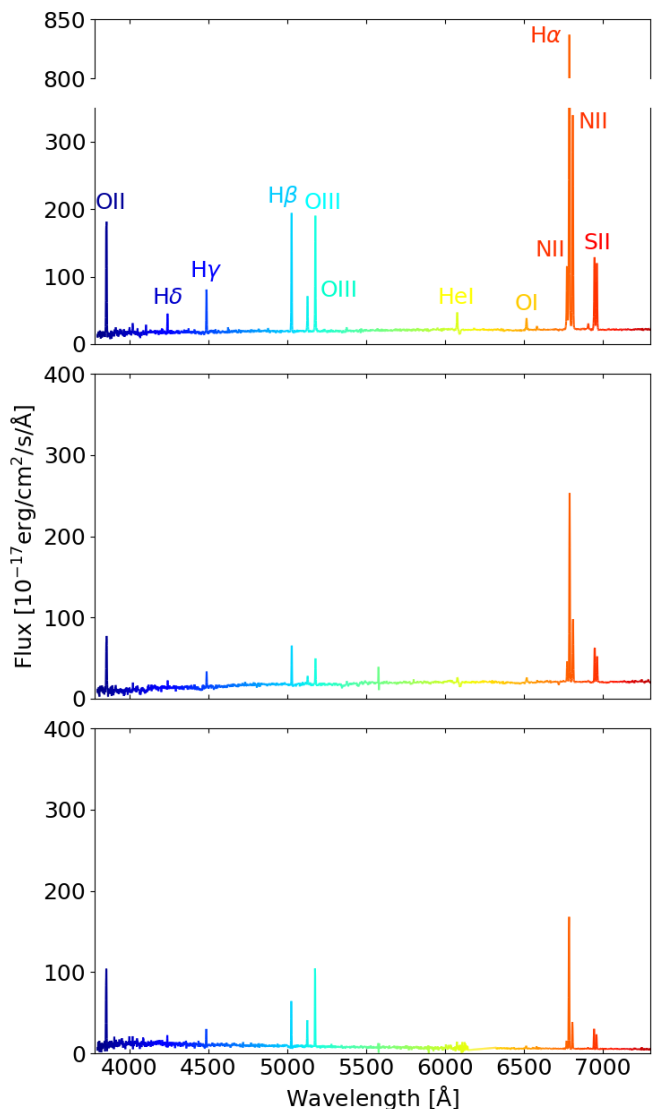


Fig. 4. SDSS optical spectra of the central region of the galaxies composing SIT 45. Each spectrum is shown for galaxy A, B, and C from upper to lower panel. Spectra are cut at 7500 Å to better show the identified emission lines.

tile range, which indicates that SIT 45 is in agreement with the distribution of σ_v for isolated triplets, in general, within 40 km s⁻¹ and 60 km s⁻¹ approximately. On the contrary, the values of R_H , H_{0t_c} , and M_{vir} for SIT 45 ($R_H = 32.38 \pm 0.03$ kpc, $H_{0t_c} = 0.0259 \pm 0.0003$, and $\log(M_{\text{vir}}) = 11.17 \pm 0.87 M_{\odot}$) are lower than the typical values in the SIT (with median values $R_H = 157.6$ kpc, $H_{0t_c} = 0.156$, and $\log(M_{\text{vir}}) = 11.65 M_{\odot}$), and even lower than the minimum value of their interquartile range. Regarding the parameters R_H and H_{0t_c} , the results suggest that SIT 45 has a more compact structure than the rest of the isolated triplets. Considering its virial mass, SIT 45 is one of the least massive triplets in the SIT, with a percentage of dark matter⁵ of about 78.6%, which is in agreement with the standard cosmological model.

⁵ The percentage of Dark Matter (DM) content is estimated using $M_{\text{vir}} = M_{\star, \text{total}} + M_{\text{DM}}$, with $M_{\star, \text{total}} = M_{\star, \text{SIT45A}} + M_{\star, \text{SIT45B}} + M_{\star, \text{SIT45C}}$, using stellar masses provided in Table 3 estimated from SED fitting (Sec. 2.2).

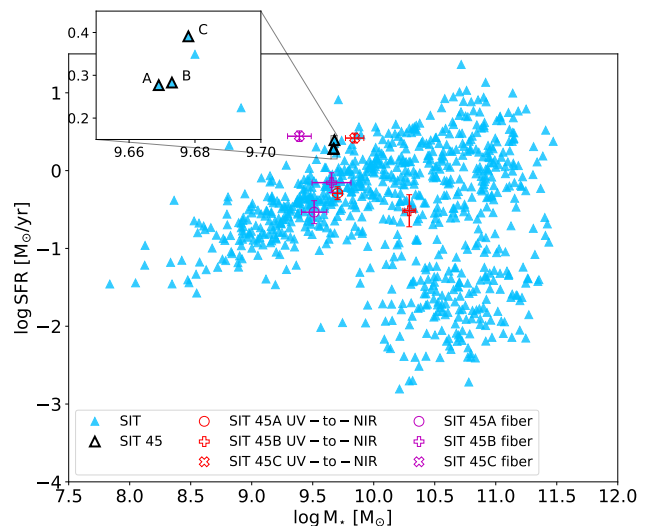


Fig. 5. Diagram of $\log(\text{SFR})$ versus $\log(M_{\star})$ for SIT galaxies in the GSWLC-M2 catalogue by Salim et al. (2018) (light blue triangles). The corresponding values for the galaxies in SIT 45 in this catalogue are represented by open black triangles. A zoom is provided to better identify the corresponding values. The values of the SFR and M_{\star} for galaxies SIT 45A, SIT 45B, and SIT 45C using SED fitting from the UV to the IR in this work are represented by red open markers according to the legend, with their corresponding errors using red error bars. We also show the values of the SFR and M_{\star} using SED fitting combining fiber photometry and spectra from the SDSS using magenta open markers according to the legend, with their corresponding errors using magenta error bars.

We also use the S parameter, defined in Eq. 8 following (Duplancic et al. 2013), to consider the compactness of the triplet. We estimated S by defining a circle, r_m , encompassing the centre of the three galaxies, finding a value of with $r_m = 55''.45$ for SIT 45. The compactness of SIT 45 is $S = 0.48 \pm 0.17$, being the maximum value for the SIT, with median $S = 0.0045$ and standard deviation $S = 0.0364$.

SIT 45 is one of the triplets with higher Q_{trip} and lower R_H and H_{0t_c} , as shown in Fig. 7. According to Vázquez-Bustos et al. (in prep.), it means that SIT 45 is a strongly interacting triplet but it does not necessarily correspond to a compact and long-term evolved system. We will discuss these results further in Sec. 4.2.

4. Discussion

4.1. Star formation history of SIT 45

To try to infer the dynamical history of SIT 45 with its assembly history, we derived physical properties as stellar age, SFR, and dust attenuation of the stellar populations for each galaxy of the triplet, using state-of-the-art UV/optical/IR SED fitting techniques. We considered photometry from GALEX, SDSS, 2MASS, and unWISE. As indicated in Sec. 2.2, we constrained the SFH assuming a delayed SFH with optional constant burst/quench event due the interaction of the member galaxies.

The resulting physical parameters of the modelled SFH with CIGALE are shown in Table 3. The second column corresponds to the obtained values of the τ_{main} parameter of the SFH. It shows that the e -folding time of the main stellar population in SIT 45B is smaller than in SIT 45A and SIT 45C, being SIT 45C the galaxy with the highest value. The values of r_{SFR} indicate recent star formation in the system. There is a burst for SIT 45B

(1)	(2)	(3)	(4)	(5)
R_H	σ_v	$H_0 t_c$	$\log(M_{\text{vir}})$	S
(kpc)	(km s^{-1})		(M_\odot)	
32.38 ± 0.03	64.43 ± 0.65	0.0259 ± 0.0003	11.17 ± 0.87	0.48 ± 0.17

Table 5. Dynamical parameters of SIT 45. The columns correspond to: (1) harmonic radius; (2) velocity dispersion; (3) crossing time; (4) virial mass; (5) compactness.

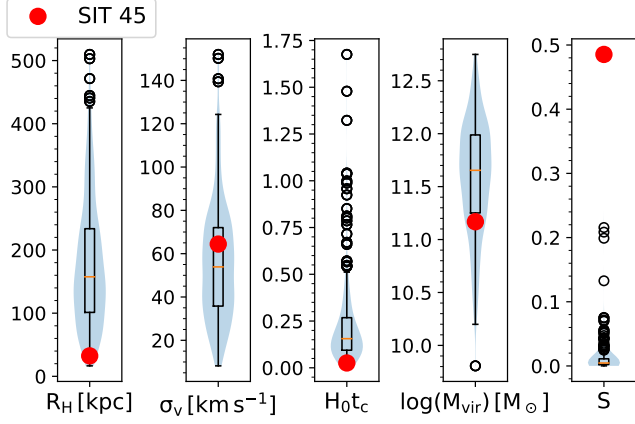


Fig. 6. Comparison of the dynamical parameters found for SIT 45 (red filled circles) with respect to the SIT. From left to right the projected harmonic radius (R_H), velocity dispersion (σ_v), crossing time ($H_0 t_c$), virial mass (M_{vir}), and compactness of the triplet (S). The pale blue violin shape corresponds to a density diagram, rotated and placed on each side, to show the form of data distribution for each dynamical parameter. The box inside the main body of the violin diagram shows the interquartile range (IQR) of the median (represented by the orange horizontal line) and its 95% confidence intervals. The vertical lines starting from the inner box correspond to $1.5 \times \text{IQR}$. The atypical values of the distribution are represented by black open circles.

and SIT 45C ~ 220 Myr ago, with a significant increase of the SFR in SIT 45C with respect to SIT 45B, which is much more modest. This event might refer to a previous encounter, leading to the tidal morphologies observed in the system. There is a recent burst episode in SIT 45A, which may have happened about 100 Myr after the encounter between SIT 45B and SIT 45C, however the uncertainty is large and it might have happened even at the same time as for galaxies SIT 45B and SIT 45C.

According to the values of the SFR, the three galaxies have ongoing star formation, with SIT 45C being the galaxy with the highest SFR. In fact, the starburst scenario for SIT 45C is supported when taking into account the stellar mass of the galaxy. In comparison with the rest of the triplets in the SIT, the SFR- M_\star diagram (presented in Fig. 5) shows that SIT 45C is located above the envelope of the star-formation main sequence, while SIT 45A and SIT 45B are located in the main sequence. These recent star-forming, with the starburst scenario for SIT 45C, are likely connected with the merging process in the system.

As expected, the uncertainties are larger in the ratio of the SFR after/before the age of the burst/quench in young burst and its age, but not so much in the stellar mass and SFR. In order to get more accurate physical parameters it is necessary to take into account other parameters to constrain the SFH, such as the H_α/H_β ratio or higher resolution IR photometry to better constrain the dust attenuation and minimise its effect in the SED modelling. While we do not have higher resolution IR photometry for the system, there are public optical SDSS spectra of the

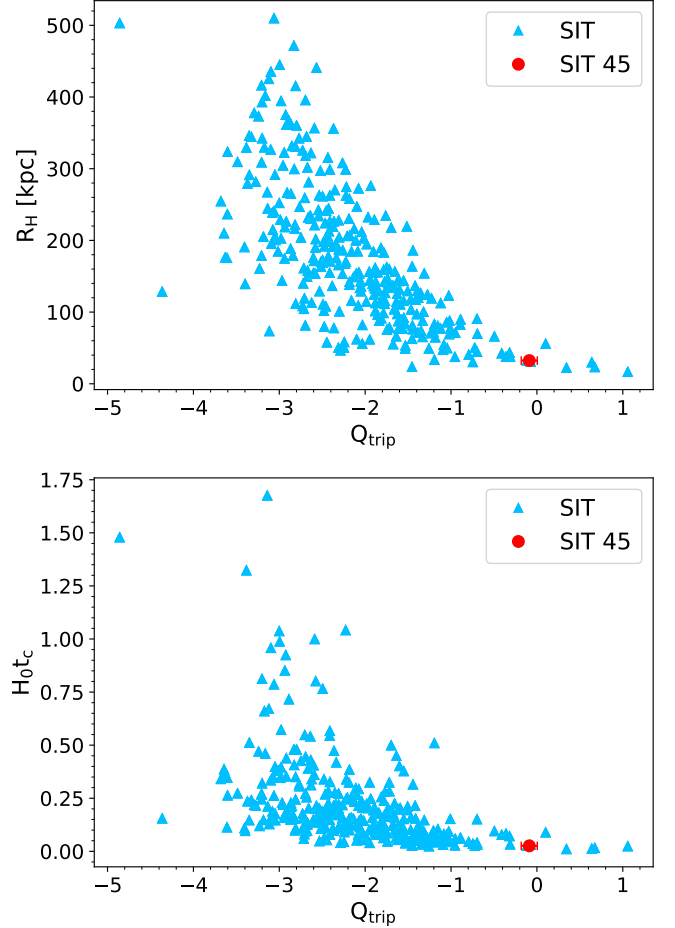


Fig. 7. Relation found of the dynamical parameters R_H (upper panel) and $H_0 t_c$ (lower panel) with the tidal strength exerted by the triplet member galaxies, Q_{trip} . The values represented by light blue triangles correspond to the values for the triplets in the SIT. The values corresponding to the isolated triplet SIT 45 are depicted by a red circle, with their corresponding errors using red error bars.

inner ($3.5''$) region of the galaxies (see Fig. 4). We have compared the obtained SFR with the SFR after considering the SDSS spectrum of each galaxy, in combination with photometry (fiber magnitudes). We also used CIGALE, which not only fits pass-band fluxes but also physical properties and can also fit emission lines fluxes. In this case we used the D4000 parameter and the H_α and H_β emission lines fluxes. We found that the resulting SFR is consistent, as shown in Table 4 and Fig. 5. The results are relatively consistent to the expected values of the SFR at fixed stellar mass according to the $D_n(4000)$ ⁶ parameter of each galaxy as presented in Duarte Puertas et al. (2022). The SFR for galaxies SIT 45B and SIT 45C are within the expected

⁶ Narrow definition of the 4000 Å break, as defined in Balogh et al. (1999), as a proxy of the main age of the stellar population.

range according to their $D_n(4000)$ values ($D_n(4000) = 1.38$, and $D_n(4000) = 1.26$, respectively, from the measurements performed in Brinchmann et al. (2004). However, as shown in Fig. 7 in Duarte Puertas et al. (2022), galaxies with younger stellar populations ($D_n(4000) < 1.2$) present higher SFR. Therefore, the expected SFR for galaxy SIT 45A ($D_n(4000) = 1.06$) should be higher than the value we have found. Overall, our results show that SIT 45 presents high values of SFR for stellar masses in the range of $8 < \log(M_*) < 11.5 M_\odot$ (as shown in Fig. 5), being therefore classified as star-forming galaxies.

According to the morphology of the galaxies in SIT 45 (blue spiral galaxies), and supported by their spectroscopic properties (star-forming galaxies), SIT 45 is therefore a major “wet” merger, i.e. a merger of similar stellar mass rich-gas blue galaxies. Our results are in agreement with Duplancic et al. (2013), where a sample of 71 triplets from the SDSS was studied. They found that blue triplets (which in general are less massive) show efficient total star-formation activity in comparison to control samples.

In general, wet mergers have been found to be more prominent in low-density environments (Bekki et al. 2001; Sánchez-Blázquez et al. 2009; Lin et al. 2010). It is important to note that we have visually inspected all the SIT triplets and we have found only 9 “wet” mergers (including SIT 45). SIT 45 is an excellent example of a triplet that might have been caught in the act of merging, before stripping and/or gas consumed to become earlier type galaxies, i.e. not so evolved. The existence of this type of systems can be considered as a consequence of the formation of structures, which occurs more slowly and on smaller scales than in regions with medium density, and a possible way for the formation of gas-rich discs (Chengalur et al. 2016). It is therefore an ideal candidate to study short time-scale mechanisms ($\sim 10^8$ years), such as interaction triggered star-formation or starbursts induced by galaxy–galaxy interactions which are more frequent at higher redshift.

We also considered the possibility of an additional scenario where SIT 45A is a tidal galaxy formed from the interaction between SIT 45B and SIT 45C. According to its SFH, there is almost no old stellar population in SIT 45A, with no detection, or very faint, in 2MASS and WISE photometry (see Fig. 2). On the contrary, the galaxy is very bright in FUV and NUV, indicating a recent (~ 100 Myr) increase of its star formation, and in line with its SFH, SIT 45A would be still forming new stars, supporting the tidal galaxy scenario. To further explore this scenario it would be necessary to perform a better SED fitting considering physical properties and emission lines, as well as an analysis of the gas-phase metallicities in extended regions, including tidal tails and bridges between galaxies SIT 45B and SIT 45C. We discarded the possibility of SIT 45A being an HII region in the tidal arm of SIT 45B. Our assumption is supported by the fact that their redshift difference even larger than the difference between SIT 45A and SIT 45C, therefore SIT 45A is not bound to SIT 45B, contrary to what is observed in HII regions (Relaño et al. 2013). Additionally, the images of the galaxy with deeper, higher resolution photometry (as Subaru HSC), shows SIT 45A as an individual galaxy, with observable different stellar populations (colours), rather than a structure of SIT 45B. This hypothesis would be easily confirmed from the kinematic analysis of SIT 45A with respect to SIT 45C, ideally using optical deep integral field spectroscopy to be able to also better constraint their SFH.

4.2. Dynamics and configuration of SIT 45

Given that SIT 45 is a merging system, we expect it to show complex dynamics. To quantify and understand its dynamical evolution we estimated its dynamical parameters R_H , σ_v , H_0t_c , and M_{vir} , described in Sec. 2.4, and presented in Sec. 3.3.

With a value of $R_H = 32.2$ kpc, SIT 45 is one of the most compact triplets in the SIT, with a median value of $R_H = 157.6$ kpc (as shown in Fig. 6). It is also more compact than triplets in other samples, with median values between $R_H = 72$ kpc and $R_H = 191$ kpc (Karachentseva & Karachentsev 2000; Makarov & Karachentsev 2000; Vavilova et al. 2005; Elyiv et al. 2009). Note that median values found for triplets are also comparable with values found in compact groups (Hickson et al. 1992; Duplancic et al. 2015). SIT 45 has a velocity dispersion $\sigma_v = 64.5$ km s $^{-1}$, which is comparable with the median value of the SIT ($\sigma_v = 53.9$ km s $^{-1}$). However, SIT triplets have lower velocity dispersion than other galaxy triplets and compact groups, which show velocity dispersion values $\sigma_v \sim 200$ km s $^{-1}$, (Duplancic et al. 2015), but the values are comparable with galaxy pairs and triplets selected by a dynamical methods (Makarov & Karachentsev 2000; Vavilova et al. 2005; Elyiv et al. 2009).

We estimated a complementary configuration parameter, the compactness S , as defined in Duplancic et al. (2013). They calculated S for a sample of galaxy triplets selected from the SDSS, and related it with their total stellar mass, obtaining values in the range $0.03 \lesssim S \lesssim 0.35$. The higher the value of S , the more compact the triplet (see Eq. 8). This parameter ranges from $S = 0.0001$ to $S = 0.48$ for the SIT, being SIT 45 the most compact isolated triplet. The estimated compactness for SIT 45 is therefore in agreement with the suggestion that it is a very compact triplet from R_H , and it seems to be even more compact than the triplets considered in Duplancic et al. (2013). However, they observed that S increases with the total stellar mass of the system, so that the blue (and therefore less massive) triplets tend to present less compact configurations. For instance, the compact isolated triplet J0848 + 1644 composed of three early-type galaxies and with $R_H = 14.6$ kpc (Feng et al. 2016) satisfies this trend. In the case of SIT 45 (composed of three low-mass blue galaxies) its high compactness might be due to its merging stage.

According to Hickson et al. (1992), the dimensionless crossing time H_0t_c is a convenient measurement of the maximum of the number of times a galaxy could have traversed the group since its formation. It is therefore an estimation of the dynamical state of a system, where systems with a long-term evolution show low values of H_0t_c . Hickson et al. (1992) found a significant correlation between crossing time (with a median value of $0.016H_0^{-1}$) and the fraction of gas-rich galaxies in compact groups, where groups with low values of H_0t_c typically contain fewer late-type galaxies. This trend might suggest that groups with low H_0t_c would be dynamically more evolved. This hypothesis agrees, for instance, with the study done by Feng et al. (2016) on the isolated compact galaxy triplet J0848 + 1644, composed of three early-type galaxies, with $H_0t_c = 0.032$. Duplancic et al. (2015) also found similar results, both from a catalogue of galaxy triplets and simulations, where the formation of early-type galaxies in evolved systems may have been favoured by galaxy mergers, in agreement with Barnes (1989) for compact groups.

Given the nature of SIT 45, composed of three blue late-type (gas rich) spirals, would not be considered as a highly evolved system, however the value of its dimensionless crossing time is one of the lowest in the SIT ($H_0t_c = 0.026$, see Table 5). This

result would imply that SIT 45 is generally more dynamically evolved compared to the SIT. However this result might be affected by the dependence of the H_{0t_c} estimation with R_H , where SIT 45 presents also a very low value with respect to the SIT, and by consequence it will show a low value of H_{0t_c} . In this sense, we also have found that these two values are somehow connected with the local environment.

In general, we have not observed a clear dependence of the dynamical parameters with the LSS environment. This result is in agreement with [Argudo-Fernández et al. \(2015b\)](#), who found that the LSS environment is less relevant than the local environment, where local neighbours typically exert about the 99% of the total tidal strength. However we do find a clear relation for R_H and H_{0t_c} with the local environment, quantified by the Q_{trip} parameter (as shown in the upper and lower panels of Fig. 7 for R_H and H_{0t_c} , respectively). High values of R_H and H_{0t_c} are restricted to systems with low values of Q_{trip} , i.e. no major tidal forces exist between triplet galaxies. In addition, isolated SIT triplets with lower values of the dynamical parameters span a wider range of Q_{trip} values, where all the systems with higher Q_{trip} (with values above -0.5 , more likely strongly interacting systems) are in the range of the lowest R_H and H_{0t_c} ([Vásquez-Bustos et al. in preparation](#)). These results contradict the findings in [Mendes de Oliveira & Hickson \(1994\)](#) for compact groups, where no correlation was found between the number of interacting galaxies and the crossing time (or group velocity dispersion).

We conclude that more dynamically evolved systems show low H_{0t_c} , but it does not necessary imply a relation in the opposite direction, it depends on the degree of the influence of the member galaxies. Therefore the observed results for SIT 45 would be connected with its ongoing merging stage rather than its dynamical evolution stage, in agreement with [Vásquez-Bustos et al. in preparation](#).

The conclusion is also supported by the dynamical mass of SIT 45, with a value of $\log(M_{\text{vir}}) = 10.6 M_{\odot}$ it is one of the least massive SIT triplets. Using the stellar mass of each galaxy in SIT 45 we have estimated a 78.6% of dark matter in the system. This value is in agreement with the standard cosmological model, which suggests that the three member galaxies might be embedded in a common dark matter halo ([Anosova et al. 1992](#); [Karachentseva et al. 2005](#)), favouring the dynamical evolution of SIT 45. The mock analysis for galaxy triplets in [Duplancic et al. \(2015\)](#) also support this assumption, where all the identified triplets have galaxy members that belong to the same dark matter halo, which is a strong evidence of the dynamical co-evolution of the system.

5. Summary and conclusions

In this work we have studied the dynamical parameters and SFH of the isolated merging galaxy triplet SIT 45. The interacting system SIT 45 (UGC 12589) is an unusual isolated triplet of galaxies, consisting of three interacting late-type galaxies. It is therefore an ideal candidate for investigating processes such as the triggering of star formation due to interaction.

To study the dynamical evolution of SIT 45 we used dynamical parameters harmonic radius R_H , velocity dispersion σ_v , crossing time H_{0t_c} , and virial mass $\log(M_{\text{vir}})$. We have explored the connection of its dynamical evolution with its local and large-scale environments, characterised by the tidal strength parameter Q and the projected local density η_k .

To relate the dynamical history of SIT 45 with its assembly history, we derived stellar age, SFR and dust attenuation of the stellar populations to constrain the SFH for each galaxy of

SIT 45, using state-of-the-art UV/optical/IR SED fitting techniques.

Our main conclusions are the following:

1. On one hand, the SIT 45 triplet is a highly isolated system with respect to its large-scale environment. On the other hand, the value of its tidal force parameter due to triplet members is one of the highest in the SIT. The system is compact as shown by its harmonic radius and compactness, which is consistent with the fact that the three galaxies that compose it are interacting.
2. According to its star formation history, the system has ongoing star-formation, with SIT 45C presenting *starburst* activity. The galaxies present recent (~ 200 Myr) star formation increase, indicating that it may have been triggered by the ongoing merging process.
3. The harmonic radius and crossing time values are much smaller than in the rest of the SIT triplets, which would suggest that the system is highly evolved. However, contrary to what would be expected, the triplet is composed of blue spirals with high star formation rate.
4. The percentage of dark matter of the triplet, estimated from its virial and stellar mass, suggests that the three member galaxies might be embedded in a common dark matter halo.
5. Taking into account these results, together with the fact that its velocity dispersion has a value similar to that of the SIT triplets, we conclude that SIT 45 is a system of three interacting galaxies that are evolving within a common dark matter halo. The isolated triplet SIT 45 is therefore an ideal candidate to study short time-scale mechanisms ($\sim 10^8$ years), such as interaction triggered star-formation or starbursts induced by galaxy-galaxy interactions which should be more frequent at higher redshift.

Considering our results, we propose two different scenarios for the formation of SIT 45A.

The analysis of the SFH from multi-wavelength SED fitting suggests the scenario where SIT 45A might be a tidal galaxy formed from the interaction between SIT 45B and SIT 45C. Tidal dwarf galaxies (TDGs) are formed of torn off material from the outer parts of a spiral disk due to tidal forces in a collision between two massive galaxies ([Braine et al. 2001](#); [Delgado-Donate et al. 2003](#)). According to numerical simulations, 25% become long-lived bound objects that typically survive more than 2 Gyr with masses above $10^8 M_{\odot}$ ([Bournaud & Duc 2006](#)). Other works suggest that TDGs have stellar masses in the range of $7.5 \leq \log(M_{\star}/M_{\odot}) \leq 9.5$ ([Duc et al. 2004](#); [Ren et al. 2020](#)). SIT 45A has an estimated mass of $\log(M_{\star}/M_{\odot}) = 9.70 \pm 0.04$, therefore is slightly above this range and would not be considered as a dwarf galaxy. However, this estimation might be overestimated given the difficulty of separating the stellar populations of SIT 45A, which overlaps with SIT 45B with respect to our line-of-sight.

Nevertheless, we also propose another scenario where the interaction between SIT 45B and SIT 45C occurs before the arrival of SIT 45A. This is consistent with the redshift differences between galaxies in the system, where SIT 45A has higher radial velocity difference with respect to SIT 45B and SIT 45C. In merging pairs, there is an excess of young stellar population directly related to the ongoing merging process ([Lambas et al. 2012](#)). However, on the other hand, galaxies in pairs with tidal features show evidence of older stellar populations that can be associated to a larger time-scale of the interaction. In this scenario, [Duplancic et al. \(2018\)](#) found enhanced star formation

indicators for galaxies in triplets that have a close companion. Therefore, the recent arrival of SIT 45A might also contribute to the increment of star formation activity, supporting this scenario.

To further explore the proposed scenarios and the kinematic mechanisms that triggered star formation in SIT 45, integral field spectroscopy observations would be necessary to allow investigating the SFR, SFH, and stellar velocity and velocity dispersion in extended regions for each galaxy. Since TDGs are found to form in massive gaseous accumulations, CO and HI observations would be necessary to study the gas component of the system. Our results point toward the necessity of developing a better understanding of the dynamics of galaxy triplets.

Acknowledgements. We thank our referee whose valuable comments have certainly contributed to improve and clarify this paper. MAF and PVB acknowledge financial support by the DI-PUCV research project 039.481/2020. MAF also acknowledges support from FONDECYT iniciación project 11200107 and the Emergia program (EMERGIA20_38888) from Consejería de Transformación Económica, Industria, Conocimiento y Universidades and University of Granada. UL and DE acknowledge support from project PID2020-114414GB-I00, financed by MCIN/AEI/10.13039/501100011033. DE also acknowledges support from Beatriz Galindo senior fellowship (BG20/00224) financed by the Spanish Ministry of Science and Innovation, and project PID2020-114414GB-I00 financed by MCIN/AEI/10.13039/501100011033. UL, SV and DE acknowledge support from project P20_00334 financed by the Junta de Andalucía and from FEDER/Junta de Andalucía-Consejería de Transformación Económica, Industria, Conocimiento y Universidades/Proyecto A-FQM-510-UGR20. MB gratefully acknowledges support by the ANID BASAL project FB210003 and from the FONDECYT regular grant 1211000. SDP is grateful to the Fonds de Recherche du Québec - Nature et Technologies and acknowledges financial support from the Spanish Ministerio de Economía y Competitividad under grants AYA2016-79724-C4-4-P and PID2019-107408GB-C44, from Junta de Andalucía Excellence Project P18-FR-2664, and also acknowledges support from the State Agency for Research of the Spanish MCIU through the ‘Center of Excellence Severo Ochoa’ award for the Instituto de Astrofísica de Andalucía (SEV-2017-0709). This research made use of ASTROPY, a community-developed core PYTHON (<http://www.python.org>) package for Astronomy (Astropy Collaboration et al. 2013); IPYTHON (Pérez & Granger 2007); MATPLOTLIB (Hunter 2007); NUMPY (Walt et al. 2011); SCIPY (Jones et al. 2001); and TOPCAT (Taylor 2005). This research made use of ASTRODENDRO, a Python package to compute dendrograms of Astronomical data (<http://www.dendrograms.org/>). This research has made use of the NASA/IPAC Extragalactic Database, operated by the Jet Propulsion Laboratory of the California Institute of Technology, in contract with the National Aeronautics and Space Administration. Funding for SDSS-III has been provided by the Alfred P. Sloan Foundation, the Participating Institutions, the National Science Foundation, and the U.S. Department of Energy Office of Science. The SDSS-III Web site is <http://www.sdss3.org/>. The SDSS-IV site is <http://www.sdss.org>. Based on observations made with the NASA Galaxy Evolution Explorer (GALEX). GALEX is operated for NASA by the California Institute of Technology under NASA contract NAS5-98034. This publication makes use of data products from the Wide-field Infrared Survey Explorer, which is a joint project of the University of California, Los Angeles, and the Jet Propulsion Laboratory/California Institute of Technology, funded by the National Aeronautics and Space Administration.

References

- Aceves, H. 2001, *MNRAS*, 326, 1412
 Agekyan, T. A. & Anosova, Z. P. 1968, *Soviet Ast.*, 11, 1006
 Aguado, D. S., Ahumada, R., Almeida, A., et al. 2019, *ApJS*, 240, 23
 Ahn, C. P., Alexandroff, R., Allende Prieto, C., et al. 2014, *ApJS*, 211, 17
 Aihara, H., Aisayyad, Y., Ando, M., et al. 2022, *PASJ*, 74, 247
 Aniano, G., Draine, B. T., Gordon, K. D., & Sandstrom, K. 2011, *PASP*, 123, 1218
 Anosova, Z. P., Kiseleva, L. G., Orlov, V. V., & Chernin, A. D. 1992, *Soviet Ast.*, 36, 231
 Araya-Melo, P. A., van de Weygaert, R., & Jones, B. J. T. 2009, *MNRAS*, 400, 1317
 Argudo-Fernández, M., Duarte Puertas, S., Ruiz, J. E., et al. 2017, *PASP*, 129, 058005
 Argudo-Fernández, M., Duarte Puertas, S., Verley, S., Sabater, J., & Ruiz, J. E. 2015a, *LSSGALPY: Visualization of the large-scale environment around galaxies on the 3D space*
 Argudo-Fernández, M., Lacerna, I., & Duarte Puertas, S. 2018, *A&A*, 620, A113
 Argudo-Fernández, M., Shen, S., Sabater, J., et al. 2016, *A&A*, 592, A30
 Argudo-Fernández, M., Verley, S., Bergond, G., et al. 2015b, *A&A*, 578, A110
 Argudo-Fernández, M., Verley, S., Bergond, G., et al. 2014, *A&A*, 564, A94
 Argudo-Fernández, M., Verley, S., Bergond, G., et al. 2013, *A&A*, 560, A9
 Astropy Collaboration, Robitaille, T. P., Tollerud, E. J., et al. 2013, *A&A*, 558, A33
 Balogh, M. L. & Morris, S. L. 2000, *MNRAS*, 318, 703
 Balogh, M. L., Morris, S. L., Yee, H. K. C., Carlberg, R. G., & Ellingson, E. 1999, *ApJ*, 527, 54
 Barnes, J. E. 1989, *Nature*, 338, 123
 Barnes, J. E. & Hernquist, L. 1992, *ARA&A*, 30, 705
 Barton, E. J., Geller, M. J., & Kenyon, S. J. 2000, *ApJ*, 530, 660
 Beers, T. C., Flynn, K., & Gebhardt, K. 1990, *AJ*, 100, 32
 Bekki, K., Couch, W. J., & Shioya, Y. 2001, *PASJ*, 53, 395
 Bergvall, N., Laurikainen, E., & Aalto, S. 2003, *A&A*, 405, 31
 Blanton, M. R., Dalcanton, J., Eisenstein, D., et al. 2001, *AJ*, 121, 2358
 Blanton, M. R. & Roweis, S. 2007, *AJ*, 133, 734
 Boquien, M., Buat, V., Burgarella, D., et al. 2022, *arXiv e-prints*, arXiv:2202.11723
 Boquien, M., Buat, V., & Perret, V. 2014, *A&A*, 571, A72
 Boquien, M., Burgarella, D., Roehly, Y., et al. 2019, *A&A*, 622, A103
 Bournaud, F. & Duc, P. A. 2006, *A&A*, 456, 481
 Braine, J., Duc, P. A., Lisenfeld, U., et al. 2001, *A&A*, 378, 51
 Brinchmann, J., Charlot, S., White, S. D. M., et al. 2004, *MNRAS*, 351, 1151
 Bruzual, G. & Charlot, S. 2003, *MNRAS*, 344, 1000
 Buat, V., Giovannoli, E., Heinis, S., et al. 2011, *A&A*, 533, A93
 Burgarella, D., Buat, V., & Iglesias-Páramo, J. 2005, *MNRAS*, 360, 1413
 Calzetti, D., Armus, L., Bohlin, R. C., et al. 2000, *ApJ*, 533, 682
 Chengalur, J. N., Pustilnik, S. A., & Egorova, E. S. 2016, *Monthly Notices of the Royal Astronomical Society*, 465, 2342
 Ciesla, L., Boselli, A., Elbaz, D., et al. 2016, *A&A*, 585, A43
 Ciesla, L., Elbaz, D., & Fensch, J. 2017, *A&A*, 608, A41
 Costa-Duarte, M. V., O’Mill, A. L., Duplancic, F., Sodr e, L., & Lambas, D. G. 2016, *MNRAS*, 459, 2539
 Coziol, R. & Plauchu-Frayn, I. 2007, *AJ*, 133, 2630
 Dale, D. A., Helou, G., Magdis, G. E., et al. 2014, *The Astrophysical Journal*, 784, 83
 de Mello, D. F., Smith, L. J., Sabbi, E., et al. 2008, *AJ*, 135, 548
 de Vaucouleurs, G., de Vaucouleurs, A., Corwin, Herold G., J., et al. 1991, *Third Reference Catalogue of Bright Galaxies*
 Delgado-Donate, E. J., Mu oz-Tu on, C., Deeg, H. J., & Iglesias-Páramo, J. 2003, *A&A*, 402, 921
 Di Matteo, P., Combes, F., Melchior, A. L., & Semelin, B. 2007, *A&A*, 468, 61
 D’Onghia, E., Mapelli, M., & Moore, B. 2008, *MNRAS*, 389, 1275
 Duarte Puertas, S., Iglesias-Páramo, J., Vilchez, J. M., et al. 2019, *A&A*, 629, A102
 Duarte Puertas, S., Vilchez, J. M., Iglesias-Páramo, J., et al. 2022, *arXiv e-prints*, arXiv:2205.01203
 Duc, P. A., Bournaud, F., & Masset, F. 2004, *A&A*, 427, 803
 Duc, P. A. & Mirabel, I. F. 1994, *A&A*, 289, 83
 Duc, P.-A. & Renaud, F. 2013, in *Lecture Notes in Physics*, Berlin Springer Verlag, ed. J. Souchay, S. Mathis, & T. Tokieda, Vol. 861, 327
 Dumont, A. & Martel, H. 2021, *MNRAS*, 503, 2866
 Duplancic, F., Alonso, S., Lambas, D. G., & O’Mill, A. L. 2015, *MNRAS*, 447, 1399
 Duplancic, F., Coldwell, G. V., Alonso, S., & Lambas, D. G. 2018, *MNRAS*, 481, 2458
 Duplancic, F., O’Mill, A. L., Lambas, D. G., Sodr e, L., & Alonso, S. 2013, *MNRAS*, 433, 3547
 Elbaz, D., Dickinson, M., Hwang, H. S., et al. 2011, *A&A*, 533, A119
 Ellison, S. L., Mendel, J. T., Scudder, J. M., Patton, D. R., & Palmer, M. J. D. 2013, *MNRAS*, 430, 3128
 Ellison, S. L., Patton, D. R., Mendel, J. T., & Scudder, J. M. 2011, *MNRAS*, 418, 2043
 Ellison, S. L., Patton, D. R., Simard, L., et al. 2010, *MNRAS*, 407, 1514
 Ellison, S. L., Viswanathan, A., Patton, D. R., et al. 2019, *MNRAS*, 487, 2491
 Elyiv, A., Melnyk, O., & Vavilova, I. 2009, *MNRAS*, 394, 1409
 Feng, S., Shao, Z.-Y., Shen, S.-Y., et al. 2016, *Research in Astronomy and Astrophysics*, 16, 72
 Gallagher, John S., I. & Ostriker, J. P. 1972, *AJ*, 77, 288
 Gao, Y. & Xu, C. 2000, *ApJ*, 542, L83
 Giovannoli, E., Buat, V., Noll, S., Burgarella, D., & Magnelli, B. 2011, *A&A*, 525, A150
 Goodman, A. A., Rosolowsky, E. W., Borkin, M. A., et al. 2009, *Nature*, 457, 63
 Gunn, J. E. & Gott, J. Richard, I. 1972, *ApJ*, 176, 1
 Heidt, J., Nilsson, K., Fried, J. W., Takalo, L. O., & Sillanp a, A. 1999, *A&A*, 348, 113
 Hern andez-Toledo, H. M., M endez-Hern andez, H., Aceves, H., & Olgu n, L. 2011, *The Astronomical Journal*, 141, 74

- Hickson, P., Mendes de Oliveira, C., Huchra, J. P., & Palumbo, G. G. 1992, *ApJ*, 399, 353
- Hunter, J. D. 2007, *Computing In Science & Engineering*, 9, 90
- Iglesias-Páramo, J. & Vilchez, J. M. 1997, *ApJ*, 489, L13
- Ji, L., Peirani, S., & Yi, S. K. 2014, *A&A*, 566, A97
- Jones, E., Oliphant, T., Peterson, P., et al. 2001, *SciPy: Open source scientific tools for Python*, [Online; accessed 2016-01-15]
- Karachentseva, V. E. & Karachentsev, I. D. 2000, *Astronomy Reports*, 44, 501
- Karachentseva, V. E., Karachentsev, I. D., & Shcherbanovskiy, A. L. 1979, *Astrofizicheskie Issledovaniia Izvestiya Spetsial'noj Astrofizicheskoy Observatorii*, 11, 3
- Karachentseva, V. E., Melnyk, O. V., Vavilova, I. B., & Makarov, D. I. 2005, *Astronomische Nachrichten*, 326, 502
- Kauffmann, G., Heckman, T. M., White, S. D. M., et al. 2003, *MNRAS*, 341, 33
- Kennicutt, Robert C., J., Keel, W. C., van der Hulst, J. M., Hummel, E., & Roettiger, K. A. 1987, *AJ*, 93, 1011
- Lambas, D. G., Alonso, S., Mesa, V., & O'Mill, A. L. 2012, *A&A*, 539, A45
- Lang, D., Hogg, D. W., & Schlegel, D. J. 2016, *AJ*, 151, 36
- Larson, R. B., Tinsley, B. M., & Caldwell, C. N. 1980, *ApJ*, 237, 692
- Lelli, F., Duc, P.-A., Brinks, E., et al. 2015, *A&A*, 584, A113
- Lin, L., Cooper, M. C., Jian, H.-Y., et al. 2010, *The Astrophysical Journal*, 718, 1158
- Lisenfeld, U., Braine, J., Duc, P. A., et al. 2004, *A&A*, 426, 471
- Lisenfeld, U., Braine, J., Duc, P. A., et al. 2002, *A&A*, 394, 823
- Makarov, D. I. & Karachentsev, I. D. 2000, in *Astronomical Society of the Pacific Conference Series*, Vol. 209, IAU Colloq. 174: Small Galaxy Groups, ed. M. J. Valtonen & C. Flynn, 40
- Martin, D. C., Fanson, J., Schiminovich, D., et al. 2005, *ApJ*, 619, L1
- Maschmann, D., Melchior, A.-L., Combes, F., et al. 2022, *A&A*, 664, A125
- McIntosh, D. H., Guo, Y., Hertzberg, J., et al. 2008, *MNRAS*, 388, 1537
- Mendes de Oliveira, C. & Hickson, P. 1994, *ApJ*, 427, 684
- Mendes de Oliveira, C., Plana, H., Amram, P., Balkowski, C., & Bolte, M. 2001, *AJ*, 121, 2524
- Moles, M., del Olmo, A., Perea, J., et al. 1994, *A&A*, 285, 404
- Moore, B., Katz, N., Lake, G., Dressler, A., & Oemler, A. 1996, *Nature*, 379, 613
- Moore, B., Lake, G., & Katz, N. 1998, *ApJ*, 495, 139
- Naab, T., Burkert, A., & Hernquist, L. 1999, *ApJ*, 523, L133
- Naab, T., Jesseit, R., & Burkert, A. 2006, *MNRAS*, 372, 839
- Neff, S. G., Thilker, D. A., Seibert, M., et al. 2005, *ApJ*, 619, L91
- Noeske, K. G., Weiner, B. J., Faber, S. M., et al. 2007, *ApJ*, 660, L43
- Noll, S., Burgarella, D., Giovannoli, E., et al. 2009, *A&A*, 507, 1793
- O'Mill, A. L., Duplancic, F., García Lambas, D., Valotto, C., & Sodré, L. 2012, *MNRAS*, 421, 1897
- Pasha, I., Lokhorst, D., van Dokkum, P. G., et al. 2021, *ApJ*, 923, L21
- Patton, D. R., Wilson, K. D., Metrow, C. J., et al. 2020, *MNRAS*, 494, 4969
- Pérez, F. & Granger, B. E. 2007, *Computing in Science and Engineering*, 9, 21
- Relaño, M., Verley, S., Pérez, I., et al. 2013, *A&A*, 552, A140
- Ren, J., Zheng, X. Z., Valls-Gabaud, D., et al. 2020, *MNRAS*, 499, 3399
- Renaud, F., Boily, C. M., Naab, T., & Theis, C. 2009, *ApJ*, 706, 67
- Renaud, F., Otero, A. S., & Agertz, O. 2022, *MNRAS*[arXiv:2209.03983]
- Reshetnikov, V., Bournaud, F., Combes, F., Faúndez-Abans, M., & de Oliveira-Abans, M. 2006, *A&A*, 446, 447
- Rosolowsky, E. W., Pineda, J. E., Kauffmann, J., & Goodman, A. A. 2008, *ApJ*, 679, 1338
- Rubin, V. C., Hunter, D. A., & Ford, W. Kent, J. 1991, *ApJS*, 76, 153
- Sabater, J., Best, P. N., & Argudo-Fernández, M. 2013, *MNRAS*, 430, 638
- Sales, L. V., Navarro, J. F., Theuns, T., et al. 2012, *MNRAS*, 423, 1544
- Salim, S., Boquien, M., & Lee, J. C. 2018, *ApJ*, 859, 11
- Salim, S., Lee, J. C., Janowiecki, S., et al. 2016, *ApJS*, 227, 2
- Salim, S., Rich, R. M., Charlot, S., et al. 2007, *ApJS*, 173, 267
- Salpeter, E. E. 1955, *ApJ*, 121, 161
- Sánchez-Blázquez, P., Gibson, B. K., Kawata, D., Cardiel, N., & Balcells, M. 2009, *MNRAS*, 400, 1264
- Skrutskie, M. F., Cutri, R. M., Stiening, R., et al. 2006, *AJ*, 131, 1163
- Sánchez-Blázquez, P., Gibson, B. K., Kawata, D., Cardiel, N., & Balcells, M. 2009, *Monthly Notices of the Royal Astronomical Society*, 400, 1264
- Tawfeek, A. A., Ali, G. B., Takey, A., Awad, Z., & Hayman, Z. M. 2019, *MNRAS*, 482, 2627
- Taylor, M. B. 2005, in *Astronomical Society of the Pacific Conference Series*, Vol. 347, *Astronomical Data Analysis Software and Systems XIV*, ed. P. Shopbell, M. Britton, & R. Ebert, 29
- Toomre, A. 1977, in *Evolution of Galaxies and Stellar Populations*, ed. B. M. Tinsley & D. C. Larson, Richard B. Gehret, 401
- Torres-Flores, S., Scarano, S., Mendes de Oliveira, C., et al. 2014, *MNRAS*, 438, 1894
- Tremonti, C. A., Heckman, T. M., Kauffmann, G., et al. 2004, *ApJ*, 613, 898
- Vavilova, I. B., Karachentseva, V. E., Makarov, D. I., & Melnyk, O. V. 2005, *Kinematika i Fizika Nebesnykh Tel*, 21, 3
- Verley, S., Leon, S., Verdes-Montenegro, L., et al. 2007, *A&A*, 472, 121
- Vogt, F. P. A., Dopita, M. A., Borthakur, S., et al. 2015, *MNRAS*, 450, 2593
- Walcher, J., Groves, B., Budavári, T., & Dale, D. 2011, *Ap&SS*, 331, 1
- Walt, S. v. d., Colbert, S. C., & Varoquaux, G. 2011, *Computing in Science & Engineering*, 13, 22
- White, J. A., Canning, R. E. A., King, L. J., et al. 2015, *MNRAS*, 453, 2718
- Wild, V., Rosales-Ortega, F., Falcón-Barroso, J., et al. 2014, *A&A*, 567, A132
- Wright, E. L., Eisenhardt, P. R. M., Mainzer, A. K., et al. 2010, *AJ*, 140, 1868
- Yasuda, N., Fukugita, M., Narayanan, V. K., et al. 2001, *AJ*, 122, 1104
- York, D. G., Adelman, J., Anderson, J. J. E., et al. 2000, *AJ*, 120, 1579
- Yuan, F.-T., Argudo-Fernández, M., Shen, S., et al. 2018, *A&A*, 613, A13
- Yuan, F. T., Takeuchi, T. T., Matsuoka, Y., et al. 2012, *A&A*, 548, A117
- Zepf, S. E. 1993, *ApJ*, 407, 448